Ninth International Conference on
THIN-WALLED STRUCTURES – ICTWS2023
Sydney, Australia, Nov 29 – Dec 1, 2023

DISTORTIONAL BEHAVIOUR, FAILURE AND DSM DESIGN OF LIPPED CHANNEL BEAMS AT ELEVATED TEMPERATURES

Natan S. Neves[*], Alexandre Landesmann[*] and Dinar Camotim[**]

* Programa de Engenharia Civil, COPPE, Universidade Federal do Rio de Janeiro, Brazil.
e-mails: natan.neves@coc.ufrj.br; alandes@coc.ufrj.br

** CERIS, DECivil, Instituto Superior Técnico (IST), Universidade de Lisboa, Portugal.
e-mail: dcamotim@civil.ist.utl.pt

Keywords: Cold-formed steel beams; Lipped channel beams; Elevated temperatures; Distortional post-buckling behaviour; Distortional failure; Shell finite element analysis; Direct Strength Method (DSM) design.

Abstract.

This work reports the results of a numerical investigation initiated by authors a few years ago [1, 2] dealing with the post-buckling behaviour, failure and Direct Strength Method (DSM) design of cold-formed steel (CFS) single-span simply supported lipped channel beams (LCB) buckling in distortional modes at elevated temperatures due to fire conditions. As done before, (i) the beams analysed display fully free end cross-section warping and wall displacement/rotation restraints, (ii) the Eurocode 3 (part 1.2) model to describe the temperature-dependence of the CFS material properties is adopted, and (iii) the results are obtained by means of ABAQUS shell finite element GMNIAs including critical-mode (distortional) initial geometrical imperfections. After presenting and discussing the main features of the beam distortional post-buckling behaviour, extensive beam distortional failure moment sets are gathered and subsequently used to develop and validate a DSM-based design approach for the beams under consideration. The proposed design approach is shown to provide a very good failure moment prediction quality, thus paving the way for the search of an efficient (safe and reliable) general DSM-based design approach capable of handling beams failing in distortional modes at elevated temperatures.

1 INTRODUCTION

Cold-formed steel (CFS) beams are highly versatile and efficient due to their adaptability and high strength-to-weight ratio. However, their inherent slenderness makes open-section thin-walled CFS beams vulnerable to several instability phenomena, namely distortional buckling. The current design specifications ensure safety against distortional failures, using the widely accepted Direct Strength Method (DSM – *e.g.*, [3-5]). This approach, included in several specifications for CFS structures [6-8], is rational and has a straightforward use, requiring only the knowledge of the member yield and buckling stresses. In this investigation, the relevant codified nominal ultimate moment is the distortional (D) one, termed M_{nD} and given by [6]

$$M_{nD} = \begin{cases} M_y + \left(1 - C_{yd}^{-2}\right)\left[M_p - M_y\right] & \lambda_D \le 0.673 \\ M_y\left[1 - 0.22/\lambda_D\right]/\lambda_D & \lambda_D > 0.673 \end{cases} \quad \text{with} \quad \lambda_D = \sqrt{\frac{M_y}{M_{crD}}} \quad , \quad (1)$$

where, (i) M_{crD} and λ_D are the beam distortional critical buckling moment and slenderness, (ii) M_y and M_p are the yield and plastic moments, and (iii) $C_{yd}=(0.673/\lambda_D)^{0.5}\le 3$ is a compression strain factor (parameter involved in the quantification of the cross-section inelastic strength reserve). Concerning the LCB distortional buckling, strength and failure, the available research work includes experimental investigations [9, 10], numerical simulations [1, 2, 11] and the development of DSM-based design proposals [2, 11-13]. It is worth noting that the currently codified DSM distortional design curve

(Eq. (1)) was calibrated on the basis of the experimental failure moment data obtained by Yu and Schafer [9], covering small-to-moderate distortional slenderness values ($0.68 \leq \lambda_D \leq 1.53$). In order to assess the accuracy of the above design curve, Martins *et al.* [2] carried out an in-depth numerical investigation on the behaviour of simply supported uniformly bent CFS beams failing in D modes. Based on the numerical failure moment data acquired, it was readily concluded that the codified DSM distortional design curve is unable to predict adequately the failure moments of a large number of simply supported beams. Indeed, these authors showed that Eq. (1) provides excessively unsafe failure moment estimates for non-stocky beams, thus confirming and extending the scope of the findings reported earlier [1], in the context of LCB under major-axis bending. Following an investigation on the mechanics of the D post-buckling buckling behaviour and failure in CFS beams, Martins *et al.* [2] proposed a novel DSM-based design curve, which was shown to perform much better than Eq. (1) for simply supported beams. This strength curve, cast in a "Winter-type" format, incorporates three parameters (*a*, *b* and *c* – equal to 0.25, 1.75 and 1.75) and reads

$$M_{nD} = \begin{cases} M_y + \left(1 - C_{yd}^{-2}\right)\left[M_p - M_y\right] & \lambda_D \leq 0.673 \\ M_y \left[1 - a/\lambda_D^b\right]/\lambda_D^c & \lambda_D > 0.673 \end{cases} \quad \text{with} \quad \lambda_D = \sqrt{\frac{M_y}{M_{crD}}} \quad . \quad (2)$$

In the context of cold-formed steel LCB uniformly bent about the major-axis under elevated temperatures, Landesmann and Camotim [1] performed a numerical investigation on the distortional post-buckling behaviour, ultimate strength and DSM design of CFS single-span simply supported beams. In order to establish some preliminary guidelines for the design of LCB under fire conditions, the authors used the numerical D failure moment data gathered to address the adequacy of the codified DSM distortional design curve in predicting simply supported LCB failure moments. They concluded that virtually all the beam distortional failure moments at elevated temperatures are overestimated by this DSM design curve (adequately modified to include the temperature effects) – the few exceptions concern stocky beams at T=200 ºC. While the DSM-based strength curve proposed by Martins *et al.* [2] succeeded in achieving a high-quality failure moment prediction for simply supported CFS beams at room temperature, its applicability to beams under elevated temperatures caused by fire conditions remains an open question – recall that elevated temperatures alter substantially the steel constitutive law, namely its Young's modulus, yield strength and amount of non-linearity.

Even if some research activity has been devoted to the behaviour and design of CFS beams at elevated temperatures (*e.g.*, [14-17]), the authors are only aware of their own previous investigation dealing with CFS beams against failing in distortional failures at elevated temperatures [1], carried out before the DSM-based strength curve set proposed by Martins *et al.* [2] was available. Therefore, the aim of this work is to assess whether this strength curve can be adopted (possibly with modifications) for beams at elevated temperatures. It presents and discusses the available results of an ongoing numerical investigation on the post-buckling behaviour, ultimate strength and DSM-based design of uniformly bent (about the major-axis) CFS simply supported LCB buckling and failing in distortional modes at (uniform) elevated temperatures, which can be as high as 800 ºC. As done in [1, 2], all the numerical distortional failure moments reported in this work (i) concern LCB containing critical-mode (D) initial imperfections with small amplitudes (10% of the wall thickness *t*) and (ii) are obtained by means of geometrically non-linear elastic-plastic shell finite element analyses (SFEA), adopting a model often used by the authors in the past. The beams analysed (i) have a wide variety of geometries (cross-section dimensions and lengths) and room-temperature yield stresses (selected to cover wide critical slenderness ranges), and (ii) are subjected to eight uniform elevated temperatures, ranging from 20/100 to 800 ºC. It should still be mentioned that some results concerning beams at room and elevated temperatures were already reported in [1] (room and elevated temperatures) – the room temperature results are shown here for validation and comparison purposes.

2 BEAM GEOMETRY SELECTION – BUCKLING BEHAVIOUR

The first task of this work consists of selecting the geometries (cross-section dimensions and lengths) of the single-span CFS LCB to be analysed. The beams analysed (i) are simply supported with respect to major and minor-axis bending, and (ii) their end cross-section have prevented torsional rotations and free warping and local displacements/rotations – see Fig. 1(a). The selection procedure involves sequences of buckling analyses, performed by means of the code GBTUL [18] or ABAQUS [19] SFEA and intended to identify beams buckling and failing in "pure" D modes – *i.e.*, such that their distortional (critical) buckling moments are well below the lowest local and global counterparts.

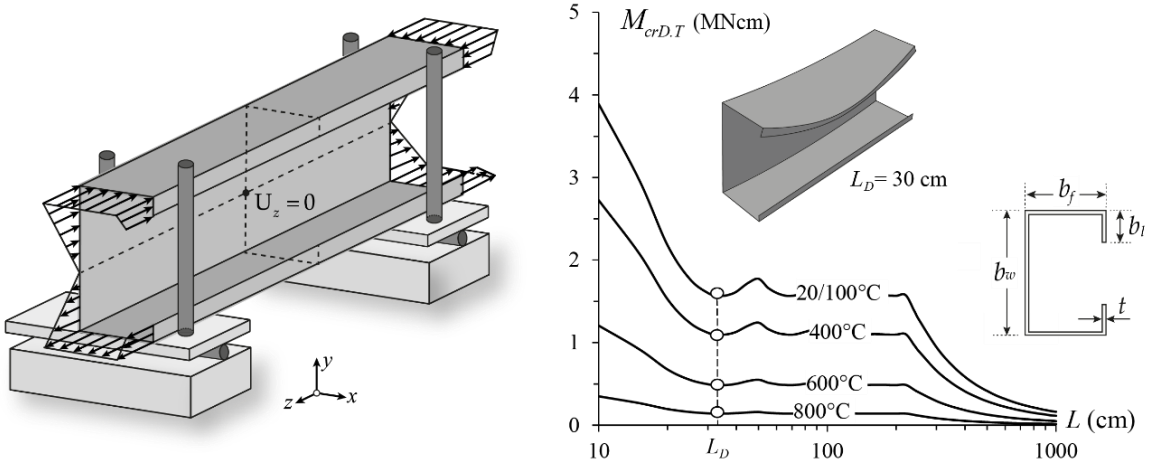

Figure 1. (a) LCB end support and loading conditions, and (b) variation of $M_{crD.T}$ with L for T=20/100-400-600-800 °C, adopting the EC3-1.2 [20] CFS temperature-dependent constitutive model.

The end product of the LCB selection procedure are the 30 cross-section dimensions (b_w, b_f, b_l and t – see Fig. 1(b)) given in Table 1. This table also provides, for each cross-section geometry, (i) the length associated with critical distortional buckling (L_D), (ii) the corresponding critical (distortional) buckling moment at room temperature (M_{crD}) and (iii) its ratios with respect to the lowest local (M_{crL}) and global (M_{crG}) buckling moments – all these buckling moments were calculated for E_{20}=210 GPa (steel Young's modulus at room temperature) and ν=0.3 (Poisson's ratio, assumed not to vary with the temperature). Note that the first "non-distortional" buckling moment is always local, with M_{crL}/M_{crD} varying from 2.2 to 2.8, and M_{crG}/M_{crD} varying from 23 to 106 (much higher). The $M_{crD.T}$ vs. L curves depicted in Fig. 1(b) provide the variation of the critical distortional buckling moment with the length L (logarithmic scale) and temperature T. Also shown is the critical (distortional) buckling mode of the LCB with L_D=30 cm. It should be pointed out that any given buckling curve can be obtained through a "vertical translation" of the top one, with a magnitude depending solely on the Young's modulus erosion stemming from the temperature rise. Moreover, the critical distortional moment $M_{crD.T}$ corresponds to the same length (L_D) for all temperature values.

3 NUMERICAL MODEL

The beam post-buckling equilibrium paths and failure moments were determined through ABAQUS [19] SFE GMNIAs, employing validated models already employed by the authors in the past (*e.g.*, [1, 2]). The beams were discretised into fine S4 element (ABAQUS nomenclature – 4-node general-purpose SFE with six degrees of freedom per node and full integration) meshes. The analyses (i) were performed by means of an incremental-iterative technique, combining Newton-Raphson's method with an arc-length control strategy, and (ii) simulate the response of beams under constant uniform temperature distributions (*i.e.*, the beams are deemed engulfed in flames, thus sharing the temperature with the surrounding air) and subsequently acted by an increasing uniform

Table 1: Selected LC beams failing in "pure" distortional modes: geometries (b_w, b_f, b_l, t, L_D – values in *mm*), critical distortional buckling moments (*kNcm*) and local-to-distortional and global-to-distortional critical moment ratios.

LCB	b_w	b_f	b_l	t	L_D	M_{crD}	$\frac{M_{crL}}{M_{crD}}$	$\frac{M_{crG}}{M_{crD}}$	LCB	b_w	b_f	b_l	t	L_D	M_{crD}	$\frac{M_{crL}}{M_{crD}}$	$\frac{M_{crG}}{M_{crD}}$
LC1	120	75	10	3	320	1788	2.7	39	LC16	120	80	10	2.5	350	1101	2.4	71
LC2	150	120	10	3.5	420	1905	2.8	106	LC17	130	80	10	2.5	400	1193	2.4	41
LC3	160	100	10	2.2	460	842	2.2	86	LC18	130	80	10	2.5	500	1331	2.2	23
LC4	200	100	10	2.5	450	1393	2.5	82	LC19	135	75	10	2.7	300	1602	2.4	52
LC5	210	70	9	2.5	340	1954	2.2	44	LC20	135	85	10	2.8	350	1493	2.6	58
LC6	210	110	10	2.5	500	1314	2.5	95	LC21	135	90	10	2.8	450	1453	2.3	41
LC7	150	95	10	2.5	400	1126	2.3	79	LC22	125	80	10	2.9	300	1639	2.4	58
LC8	150	100	10	2.5	450	1062	2.4	75	LC23	125	80	10	2.9	400	1655	2.4	32
LC9	150	75	10	2.5	400	1468	2.4	34	LC24	160	90	10	2.5	400	1267	2.5	66
LC10	150	80	10	2.5	400	1359	2.5	43	LC25	165	85	10	2.4	400	1261	2.5	58
LC11	130	80	10	3	350	1803	2.6	42	LC26	250	100	12	2.8	500	2591	2.4	56
LC12	130	80	10	3	400	1848	2.5	32	LC27	275	110	13	3	550	3204	2.4	58
LC13	140	90	10	2.5	350	1145	2.3	81	LC28	265	105	13	3	550	3253	2.4	49
LC14	145	90	10	2.45	450	1115	2.4	52	LC29	215	80	10	2.8	400	2477	2.5	42
LC15	150	100	10	2.5	450	1062	2.4	75	LC30	225	90	12	2.9	450	2845	2.5	44

major-axis bending moment up to failure – steady-state structural analyses providing failure moments. Note that, in the context of the distortional ultimate strength of CFS columns, it has been shown in the past (*e.g.*, [21]) that the failure loads provided by steady-state analyses match the more realistic failure temperatures obtained through the "corresponding" transient analyses – axially compressed columns heated up to failure. It is assumed here that the above finding can be extended to beams, *i.e.*, that the failure moments provided by steady-state analyses match the failure temperatures obtained from the transient analyses.

The simply supported beams analysed are depicted in Fig. 1(a) – note that, in order to preclude the occurrence of rigid-body motions, the longitudinal displacement at the mid-span cross-section mid-web point is prevented in all the beams analysed. The uniform bending moment diagram is applied by means of sets of concentrated forces acting on the nodes of both end cross-sections. The force/moment application is always imposed in small increments, by means of the ABAQUS automatic loading stepping procedure. All the beams analysed contain initial geometrical imperfections with the critical-mode (D) shape and small amplitudes (0.1t). These initial imperfections involve inward compressed flange-lip motions, since they have been shown to be the most detrimental, in the sense that they lead to lower post-buckling strengths [1, 2]. The beam critical buckling mode shapes were obtained through preliminary ABAQUS buckling analyses, performed with the same SFE mesh subsequently employed to carry out the GMNIA. It is still worth noting that strain-hardening, residual stress and rounded corner strength effects were disregarded in this work, since it has been shown (*e.g.*, [22]) that their joint influence on the failure moments is negligible. The multi-linear stress-strain curve available in ABAQUS is adopted to model the steel material behaviours associated with the several yield stresses considered. The CFS constitutive law at elevated temperature adopted in this work is that prescribed in EC3:1-2 [20], which was previously adopted in the numerical simulations reported in [1, 23].

4 DISTORTIONAL RESPONSE UNDER ELEVATED TEMPERATURES

4.1 Elastic-Plastic Post-Buckling Behaviour

The influence of the (elevated) temperature on the distortional elastic-plastic post-buckling behaviour and failure moment of selected CFS lipped channel beams is addressed in this section. The investigation deals with the LC19 geometry (see Table 1) and adopts the EC3-based temperature-dependent steel constitutive model – the results presented and discussed constitute a representative sample of the whole set of beams dealt with in this work. Fig. 2(a) shows M/M_{crD} vs. $|v|/t$ equilibrium paths (t is the wall thickness and $|v|$ is the absolute value of the beam maximum vertical displacement, occurring at the mid-height compressed/top flange-lip corner) of beams with λ_D=1.2 (yield stress $\sigma_{y.20}$ equal to 600 MPa) under temperatures T=20/100-200-300-400-500-600-700-800 ºC. The white circles identify the failure moments $M_{u.T}$ and the room temperature elastic curves are also shown, for comparison purposes. As for Fig. 2(b), it displays the deformed configurations and von Mises stress contours, at collapse (M=$M_{u.T}$), of the beam under temperatures T=20/100-300-600-800 ºC. The observation of these post-buckling results prompts the following remarks:

(i) As expected, the beam normalised strength and failure moment decrease as the temperature T rises. The drop is mostly perceptible between 500 and 600 ºC.

(ii) The equilibrium paths of the beams under temperatures T≥600 °C are clearly below the remaining ones, thus reflecting the sudden increase in the rate of the steel material behaviour erosion occurring between 500 and 600 °C. This erosion is mostly felt via the proportionality limit strain and the smoothness of the elliptic transition between the elastic and plastic ranges. For T>600 °C, the steel stress-strain curve exhibits again a well-defined yield plateau.

(iii) Concerning the beam failure modes (deformed configurations at collapse), it is worth noting that, since the thermal action effects are negligible (uniform temperature and free-to-deform beams), they do not vary with the temperature – indeed, they virtually coincide for all the beams analysed. This is also true for the corresponding von Mises stress contours – the beams always collapse after the full yielding of the top (compressed) web-flange corners and lip free edge at the mid-span region, leading to the formation of a "distortional plastic hinge" – similar observations were reported in [1, 2]. In quantitative terms, the stresses obviously decrease as the temperature rises and continuously erodes the steel material behaviour.

(iv) No clear trend was detected concerning the influence of the temperature, geometry and/or steel grade on the amount of elastic-plastic strength reserve and ductility prior to failure. Moreover, all the beams analysed exhibit quite similar post-collapse behaviours (equilibrium path descending branches), regardless of the temperature.

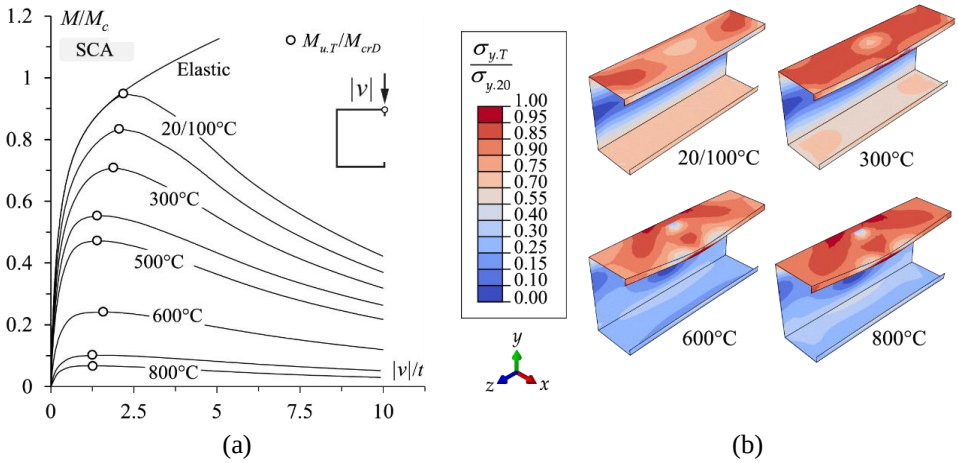

(a) (b)

Figure 2. LC19 beams with λ_D=1.2 and under elevated temperatures: distortional (a) post-buckling equilibrium paths M/M_{crD} vs. $|v|/t$ and (b) deformed configurations and von Mises stress contours at collapse.

4.2 Failure Moment Data

This section reports the output of a parametric study carried out to gather the failure moment data that will be used to develop and assess the merits of a DSM-based design approach intended to handle lipped channel beam buckling and failing in distortional modes at elevated temperatures. This parametric study involves a total of 1200 beams, corresponding to all possible combinations of (i) the 30 geometries (cross-section dimensions and lengths) given in Table 1, (ii) 8 uniform temperatures (T=20/100-200-300-400-500-600-700-800 ºC) and (iii) 5 yield stresses at room temperature. The whole set of numerical results obtained is given in [24]. Fig. 3 shows plots $M_{u.T}/M_{y.T}$ *vs.* $\lambda_{D.T}$ for the various temperatures considered in this work, each of them including, for comparison purposes, the elastic buckling curves $(1/\lambda_{D.T})^2 - M_{u.T}$, $M_{y.T}$ and $\lambda_{D.T}=(M_{y.T}/M_{crD.T})^{0.5}$ are the beam distortional failure moments, yield moments and slenderness values, respectively. Besides the failure moment data obtained in this work, Fig. 3 includes also 510 numerical D failure moments reported in [1] (room and elevated temperatures), respectively. The joint observation of these various plots leads to the following comments:

(i) Regardless of the temperature, the $M_{u.T}/M_{y.T}$ *vs.* $\lambda_{D.T}$ "clouds" follow the trend of "Winter-type" strength curves, even if there exists some "vertical dispersion" along the whole slenderness ranges considered, thus reflecting the influence of the beam cross-section geometry on the beam distortional post-critical strength reserve (see [2] in the context of D beams at room temperature).

(ii) It is quite interesting to notice that, for $\lambda_{D.T}\geq 1.5$ and regardless of the temperature, the elastic buckling strength curves provide lower bounds for all the $M_{u.T}/M_{y.T}$ values.

(iii) All the $M_{u.T}/M_{y.T}$ values concerning stocky beams at temperatures $T>200$ ºC are well below 1.0, in clear contrast with what happens for $T\leq 200$ ºC – the differences tend to increase with the temperature and the elastic buckling curves provide a useful reference to quantify them. In the moderate and high slenderness ranges ($\lambda_{D.T}>0.673$), this very striking distinction between the $M_{u.T}/M_{y.T}$ values concerning the beams at $T>200$ ºC and $T\leq 200$ ºC ceases to occur.

(iv) Concerning the stocky beams at $T>200$ ºC, note that their $M_{u.T}/M_{y.T}$ values are aligned along clearly descending curves branches that transition fairly smoothly to those associated with the beams exhibiting moderate and high slenderness values. Moreover, note also that these "stocky beam $M_{u.T}/M_{y.T}$ curves" originate at points ($M_{p.T}$) not ordered according to the temperature value – this stems from the fact that the k_p/k_y values prescribed for CFS in EC3-1.2 are not "logically ordered", since they are equal to 1-0.907-0.786-0.646-0.679-0.6-0.577-0.714.

(v) The results displayed in Fig. 3 clearly show that the failure moment predictions for beams at $T>200$ ºC and $T\leq 200$ ºC must be handled separately in the low-to-moderate slenderness range (at least when the EC3-based CFS constitutive model is adopted). The quantification of these qualitative assertions is addressed in the next section.

5 DSM DESIGN AT ELEVATED TEMPERATURES

The DSM-based prediction of the D failure moments gathered in Section 4.2, concerning CFS simply supported LCB at elevated temperatures, is addressed in this section. The first step consists of assessing the adequacy of the most performant DSM-based design approach available to handle beam distortional failures at room temperature, namely Eq. (2) with the values of *a*, *b* and *c* proposed in [2]. Naturally, these strength curves must be appropriately adapted to include the temperature effects associated with the EC3:1-2 [20] material model, via the D buckling ($M_{crD.T}$), yield ($M_{y.T}$) and plastic ($M_{p.T}$) moments, which implies that λ_D and C_{yd} will also vary with T (they become $\lambda_{D.T}$ and $C_{yd.T}$). It should be noted that this approach was already explored by other authors (*e.g.*, Bandula Heva and Mahendran [25] and Bicelli *et al.* [26], for columns buckling and failing in flexural-torsional modes, and Landesmann *et al.* [27], for columns buckling and failing in distortional modes). Thus, the nominal estimates of the beam distortional failure moments at elevated temperatures are provided by

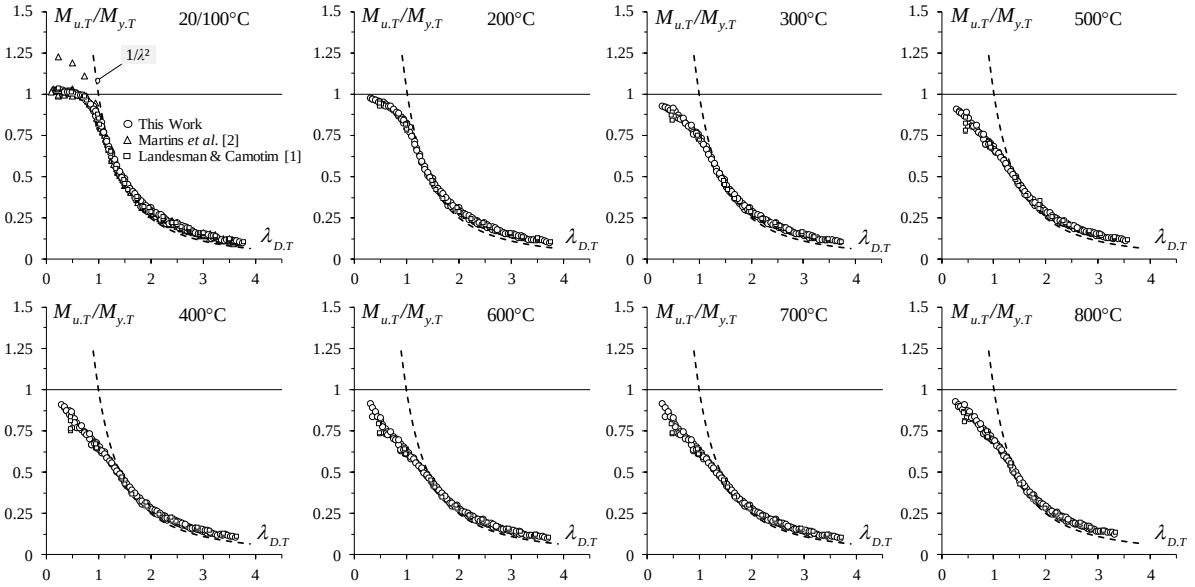

Figure 3. $M_{uT}/M_{y.T}$ *vs.* $\lambda_{D.T}$ values concerning all the LC beams under room and elevated temperatures analysed in this work and elastic buckling curves (T=20/100-200-300-400-500-600-700-800 ºC).

$$M_{nD.T}=\begin{cases} M_{y.T}+\left(1-C_{yd.T}^{-2}\right)\left[M_{p.T}-M_{y.T}\right] & \lambda_{D.T}\le 0.673 \\ M_{y.T}\left[1-a/\lambda_{D.T}^{b}\right]/\lambda_{D.T}^{c} & \lambda_{D.T}>0.673 \end{cases} \quad \text{with} \quad \lambda_{D.T}=\sqrt{\frac{M_{y.T}}{M_{crD.T}}} \quad , \quad (3)$$

where it should be noted that, with respect to Eq. (2), (i) the compression strain factor C_{yd} (quantifying the inelastic strength reserve) becomes temperature-dependent ($C_{yd.T}=(0.673/\lambda_{D.T})^{0.5}\le 3$) and (ii) the values of parameters *a*, *b* and *c* proposed in [2] are deemed not vary with the temperature. The plots $M_{u.T}/M_{nD.T}$ *vs.* $\lambda_{D.T}$, shown in Fig. 4 and concerning the LCB analysed in this work and reported in [1], enable a quick and visual qualitative assessment of the quality (accuracy and safety) of the failure moment predictions provided by Eq. (3). The observation of the results presented in these figures prompts the following comments:

(i) A distinction must be made between the beams at $T\le 300$ ºC and $T\ge 400$ ºC. For the former, the failure moment predictions provided by Eq. (3) are (i_1) safe and accurate for $\lambda_{D.T}>1.0$ (only a few slightly unsafe predictions and all underestimations below 9%) and (i_2) consistently unsafe for $\lambda_{D.T}\le 1$, even if the overestimations never exceed 19% – they become more pronounced for T=300 ºC. For the beams under $T\ge 400$ ºC, the D slenderness threshold separating the safe and unsafe failure moment estimates moves from $\lambda_{D.T}$=1.0 to $\lambda_{D.T}$=1.5. Regardless of the temperature, (i_1) the "safe slenderness range" continues to be characterised by only a few slightly unsafe failure moment estimates and fairly small underestimations (all below 15%, with most of them not exceeding 10%), while (i_2) the "unsafe slenderness range" now exhibits visibly larger failure moment overestimations, which can be as high as 30%.

(ii) In view of the content of the previous item, it can be concluded that the DSM-based strength curve $M_{nD.T}$ predicts quite satisfactorily the failure moments of the LCB in the moderate-to-high slenderness range ($\lambda_{D.T}>1.0$ or $\lambda_{D.T}>1.5$, respectively for $T\le 300$ ºC and $T\ge 400$ ºC).

(iii) Therefore, it is clear that, in order to improve the failure moment prediction quality provided by the DSM-based design curve $M_{nD.T}$ for LCB under elevated temperatures, this strength curve needs to be modified/lowered in the low-to-moderate slenderness range. A possible modification is proposed in the next section, which also includes the assessment of the failure moment prediction quality it entails – the reliability of the modified DSM-based design approach is also addressed.

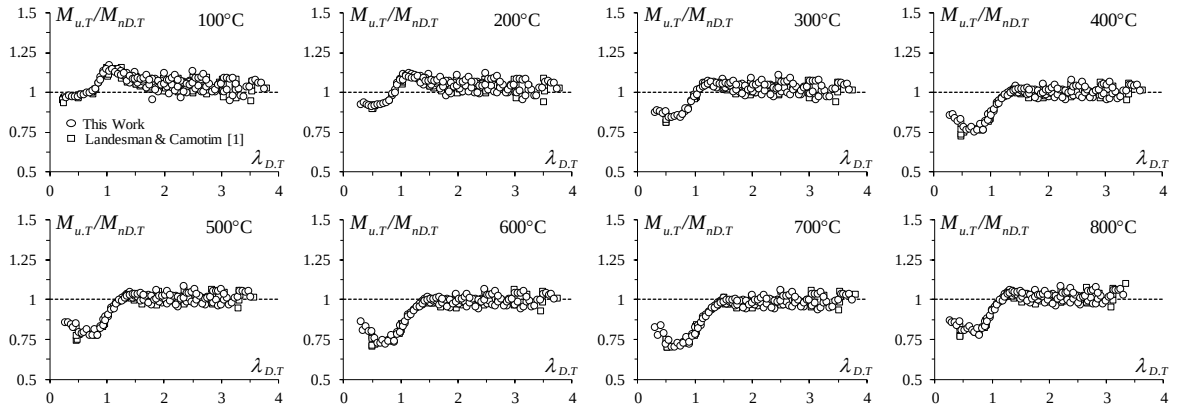

Figure 4. $M_{u.T}/M_{nD.T}$ *vs.* $\lambda_{D.T}$ plots for the LCB analysed in this work and reported in [1] (T=20/100 ºC to T=800 ºC).

5.1 Modification of the available DSM-based design curves at elevated temperatures

In order to improve the failure moment prediction quality provided by Eq. (3) for the LCB exhibiting low and moderate slenderness values, the strategy previously employed by other authors (*e.g.*, [24, 25]) is adopted in this work. It consists of modifying/lowering Eq. (3) by incorporating the reduction factor ratios k_p and k_y, which were shown earlier to play a key role in the steel constitutive law temperature-dependence prescribed by the EC3-1.2 model [20] (see Section 4.2). The proposed modification involves (i) replacing $M_{y.T}$ (yield moment at elevated temperatures) with $M_{y.20}\cdot k_p$, where it should be recalled that $k_p=\sigma_{p.T}/\sigma_{y.20}$ ($\sigma_{p.T}$ is the proportionality limit stress at temperature T), (ii) including the coefficient $(k_p/k_y)^{2.5}$ in the design curve first branch (see the first expression in Eq. (4)), (iii) replacing the parameter a with $[a\cdot(k_y/k_p)]$ in the design curve second branch (see the second expression in Eq. (4)), and (iv) replacing the distortional slenderness transition value 0.673 with $0.673/\eta$, where $\eta\leq 1.0$ is a coefficient calculated to ensure continuity of the design curves – its values are given, for the eight temperature values considered in this work, in the table appearing in Fig. 5(b) – linear interpolation can be used to obtain the η values concerning intermediate temperatures. The modified/lowered DSM-based design curve, denoted $M_{nD.T*}$, is given by the expressions

$$M_{nD.T*}=\begin{cases}\left(M_{y.20}\cdot k_p\right)+\dfrac{\left(1-C_{yd.T}^{-2}\right)}{\left(k_p/k_y\right)^{2.5}}\left[M_{p.T}-M_{y.T}\right] & \lambda_{D.T}\leq 0.673/\eta \\ M_{y.T}\left[1-a\cdot\left(k_y/k_p\right)/\lambda_{D.T}^{b}\right]/\lambda_{D.T}^{c} & \lambda_{D.T}>0.673/\eta\end{cases} \quad \text{with} \quad \lambda_{D.T}=\sqrt{\frac{M_{y.T}}{M_{crD.T}}} \quad , \quad (4)$$

where (i) $C_{yd.T}=(0.673\eta^{-1}/\lambda_{D.T})^{0.5}\leq 3$, (ii) k_p and k_y are the proportional limit and yield stress reduction factors prescribed in EC3-1-2 [20]), and (iii) the values of parameters a, b and c are those proposed in [2], deemed not vary with the temperature.

Figure 5(a) displays the DSM-based design curves defined by Eq. (4) – it includes a zoomed view of the transition between the pairs of design curve branches. It is worth noting that (i) the design curves remain unchanged for the room/mildly elevated temperature ($T\leq$100 ºC – $\eta=k_p=k_y=1$) and (ii) the modifications of the design curves concerning the elevated temperatures are only felt in the low-to-moderate slenderness range ($\lambda_{D.T}\leq 0.673/\eta$) – the failure moment predictions concerning LCB such that $\lambda_{D.T}>0.673/\eta$ remain practically unaltered. Since the design curve modifications stem essentially from the incorporation of the ratio k_p/k_y, it is just logical to expect the temperature-dependence of this ratio to be directly reflected in the design curve variation with the temperature. Indeed, this is the case: as clearly shown in Fig. 5(a), the modified design curves are ordered like the k_p/k_y values – sequence T=20/100-200-300-800-500-400-600-700 ºC.

In order to enable the qualitative assessment of the failure moment prediction quality provided by Eq. (4), Fig. 6 shows the $M_{u.T}/M_{nD.T*}$ *vs.* $\lambda_{D.T}$ plots concerning the whole set of LCB analysed in this

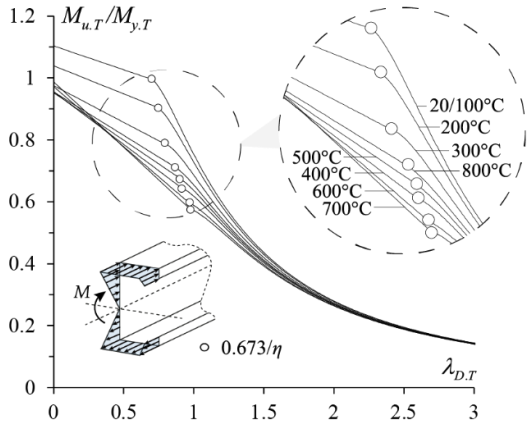

T (ºC)	η
20/100	1.00
200	0.92
300	0.84
400	0.74
500	0.75
600	0.70
700	0.69
800	0.78

(a) (b)

Figure 5. (a) $M_{nD.T^*}$ DSM-based D strength curves and (b) values of η for LCB under elevated temperatures.

work and in [1] – the full set of $M_{u.T}/M_{nD.T^*}$ values for LCB analysed in this work and reported in [1] are given in [27]. The observation and analysis of the results presented in Fig. 6, as well as their comparison with those previously displayed in Fig. 4, prompt the following remarks:

(i) It is clear that the proposed modification of Eq. (3), leading to Eq. (4), considerably improves the failure moment prediction quality for LCB with low and moderate slenderness values (*i.e.*, such that $\lambda_{D.T} \leq 0.673/\eta$) at elevated temperatures. Moreover, it is also very clear that, regardless of the slenderness and temperature values, Eq. (4) yields quite good failure moment estimates for all the LCB considered, *i.e.*, either analysed in this work or reported in [1].

(ii) The $M_{u.T}/M_{nD.T^*}$ statistical indicators (see [27]), which are similarly good for all the temperatures considered, confirm the above assertion – the averages, standard deviations and maximum-minimum values for LCB with $\lambda_{D.T} \leq 0.673/\eta$ vary from 0.97 to 1.06, 0.01 to 0.05, 0.99 to 1.20, and 0.89 to 0.97. Moreover, the numbers of "clearly unsafe" failure moment estimates concerning the LCB with $\lambda_{D.T} \leq 0.673/\eta$ are now quite small – 14 (out of 160 – 8.8%). For the LCB with $\lambda_{D.T} > 0.673/\eta$, these numbers are much smaller: they read 5 (out of 1355 – 0.4%). On the other hand, it should also be noted that the maximum and minimum predicted-to-numerical failure moment ratios are equal to 1.20 and 0.90, respectively.

(iii) The very good performance of Eq. (4) in predicting the failure moments of LCB provides encouragement to proceed along this path in the search for an efficient DSM-based design approach capable of handling the D failures of cold-formed steel beams at elevated temperatures.

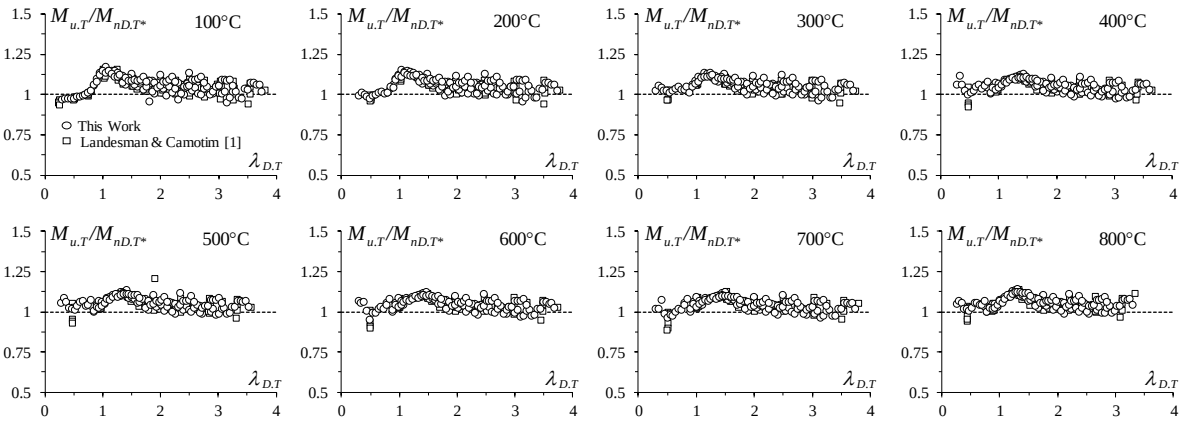

Figure 6. $M_{u.T}/M_{nD.T^*}$ *vs.* $\lambda_{D.T}$ plots for the LCB beams analysed in this work and in [1] (T=20/100-800ºC).

5.2 Reliability Assessment

Next, the reliability of the failure moment predictions provided by the proposed DSM-based design approach is assessed, through the determination of the LRFD (Load and Resistance Factor Design) resistance factors ϕ associated with the numerical failure moments obtained for the CFS LC beams analysed in this work and in [1]. In particular, it is intended to check whether values equal to or higher than ϕ_b=0.90 are achieved – this is the limit value prescribed by the current North American Specification [6] for members subjected to bending.

The ϕ values obtained from the $M_{nD.T^*}$ failure moment estimates concerning the LCB at T=20/100-200-300-400-500-600-700-800 ºC are not far apart from each other, regardless of the temperature considered – indeed, they read 0.952-0.961-0.961-0.959-0.961-0.954-0.961-0.964. In addition, it should also be noted that all of these ϕ values are visibly above that prescribed in [6] for members in bending (ϕ_b=0.90). If the $M_{nD.T^*}$ failure moment estimates concerning all the temperature values considered are put together, the ϕ value obtained is 0.956 – visibly above ϕ_b=0.90. Therefore, it seems fair to conclude that the proposed DSM-based design approach ($M_{nD.T^*}$) handles reliably cold-formed steel LCB failing in distortional modes, both at room and elevated temperatures.

6 CONCLUDING REMARKS

This paper reported the most recent results of an investigation, initiated a few years ago [1, 2], on the post-buckling behaviour, ultimate strength and DSM design of cold-formed steel single-span simply supported lipped channel beams buckling in distortional modes at room and elevated temperatures, typically caused by fire conditions. The numerical distortional failure moments obtained in this work, together with those previously reported in [1], were subsequently used to propose a contribution towards the development of an efficient DSM-based design approach for cold-formed steel beams failing in distortional modes at room and elevated temperatures. Out of the various findings reported in this work, the following ones deserve to be specially mentioned:

(i) It was shown that incorporating the temperature dependence of the critical distortional buckling ($M_{crD.T}$), yield ($M_{y.T}$) and plastic ($M_{p.T}$) moments in the DSM-based design curve proposed in [2] does not lead to an acceptable failure moment prediction quality for LCB at elevated temperatures. Indeed, regardless of the temperature, safe and reasonably accurate failure moment estimates are only obtained for beams with a fairly high slenderness – in the low and moderate slenderness range, several LCB failure moments are clearly overestimated, thus providing ample evidence that the above DSM-based design curve needs to be modified.

(ii) The DSM-based distortional design curve addressed in the previous item was modified through the inclusion of (ii$_1$) the temperature-dependent ratio k_p/k_y, where k_p and k_y are reduction factors prescribed in [20], and (ii$_2$) the coefficient η, calculated to ensure continuity between the branches of the two (modified) design curves. In spite of its simplicity, this modification led to a quite considerable improvement in failure moment prediction quality for LCB exhibiting low and moderate distortional slenderness at elevated temperatures.

(iii) The failure moment predictions provided by the (modified) DSM-based distortional design curve proposed, for the lipped channel beams at room and elevated temperatures analysed in this work and in [1], lead to LRFD resistance factors never below 0.952, *i.e.*, well above the value prescribed in AISI [6] for members subjected to bending – ϕ_b=0.90.

REFERENCES

[1] Landesmann A, Camotim D (2016). Distortional failure and DSM design of cold-formed steel lipped channel beams under elevated temperatures, *Thin-Walled Structures*, **98A**(January), 75-93.

[2] Martins AD, Landesmann A, Camotim D, Dinis PB (2017). Distortional failure of cold-formed steel beams under uniform bending: Behaviour, strength and DSM design, *Thin-Walled Structures*, **118**(September), 196-213.

[3] Camotim D, Dinis PB, Martins AD (2016). Direct Strength Method (DSM) – a general approach for the design of cold-formed steel structures, *Recent Trends in Cold-Formed Steel Construction*, C. Yu (ed.), Woodhead Publishing (Series in Civil and Structural Engineering), Amsterdam, 69-105

[4] Schafer BW (2019). Advances in the Direct Strength Method of cold-formed steel design, *Thin-Walled Structures*, **140**(July), 533-541.

[5] Camotim D, Martins AD, Dinis PB (2023). Towards the next generation design of cold-formed steel structures: the Direct Strength Method (DSM), *Recent Trends in Cold-Formed Steel Construction* (2nd ed.), C. Yu (ed.), Elsevier, Amsterdam, *in press*.

[6] AISI (American Iron and Steel Institute) (2022). *North American Specification (NAS) for the Design of Cold-Formed Steel Structural Members* (2016 edition reaffirmed in 2020 with Supplement 3), AISI-S100-16 w/S3-22, Washington DC.

[7] AS/NZS (Standards of Australia and Standards of New Zealand) (2018). *Cold-Formed Steel Structures*, AS/NZS 4600:2018 (3rd ed.), Sydney-Wellington.

[8] ABNT (Brazilian Standards Association) (2010). *Brazilian Standard on Design of Cold-Formed Steel Structures*, (ABNT NBR 14762:2010, Rio de Janeiro. (Portuguese).

[9] Yu C, Schafer BW (2006). Distortional buckling tests on cold-formed steel beams, *Journal of Structural Engineering* (ASCE), **132**(4), 515-528.

[10] Wang L, Young B (2014). Design of cold-formed steel channel with stiffened webs subjected to bending, *Thin-Walled Structures*, **85**(December), 81-92.

[11] Yu C, Schafer BW (2007). Simulation of cold-formed steel beams in local and distortional buckling with applications to the direct strength method, *Journal of Constructional Steel Research*, **63**(May), 581-590.

[12] Schafer BW, Peköz T (1998), Direct strength prediction of cold-formed steel members using numerical elastic buckling solutions, *Proceedings of 14th International Specialty Conference on Cold-Formed Steel Structures* (St. Louis, 15-16/10), W.W. Yu, R. Laboube (eds.), 69-76.

[13] Schafer BW (2008), Review: the direct strength method of cold-formed member design *Journal of Constructional Steel Research*, **64**(7-8) (2008), 766-778.

[14] Kankanamge ND, Mahendran M (2012). Behaviour and design of cold-formed steel beams subject to lateral–torsional buckling at elevated temperatures, *Thin-Walled Structures*, **61**(December), 213-228.

[15] Laím L, Rodrigues JPC, Craveiro HD (2016). Flexural behaviour of axially and rotationally restrained cold-formed steel beams subjected to fire, *Thin-Walled Structures*, **98A**(January), 39-47.

[16] Laím L, Rodrigues JPC (2018). Fire design methodologies for cold-formed steel beams made with open and closed cross-sections, *Engineering Structures*, **171**(September), 759-778.

[17] Santiago IB, Rodrigues JPC, Rodrigues FC, de Oliveira RLG (2021). Numerical analysis of cold-formed steel sigma-shaped beams in fire conditions, *Architecture, Structures and Construction*, **1**(September), 53-63.

[18] Bebiano R, Camotim D, Gonçalves R (2018). GBTUL 2.0 – a second-generation code for the GBT-based buckling and vibration analysis of thin-walled members, *Thin-Walled Structures*, **124**(March), 235-257.

[19] Simulia Inc. (2014). *ABAQUS Standard* (version 6.14-1).

[20] CEN (Comité Européen de Normalisation) (2005). *Eurocode 3: Design of Steel Structures – Part 1.2: General Rules – Structural Fire Design*, EN 1993-1-2, Brussels.

[21] Landesmann A, Camotim D (2011). On the distortional buckling, post-buckling and strength of cold-formed steel lipped channel columns under fire conditions, *Journal of Structural Fire Engineering*, **2**(1), 1-19.

[22] Ellobody E, Young B (2005). Behavior of cold-formed steel plain angle columns, *Journal of Structural Engineering* (ASCE), **131**(3), 469-478.

[23] Arrais F, Lopes N, Real PV (2021). Fire design of slender cold-formed lipped channel and sigma section members with uniform temperature under compression, *Fire Safety Journal*, **122**(June), paper 103340 (17 pages).

[24] Neves NS, Landesmann A, Camotim D (2023). CFS lipped channel beams buckling in distortional modes at elevated temperatures: behaviour, failure and DSM design, *submitted for publication*.

[25] Bandula Heva Y, Mahendran M (2012). Flexural-torsional buckling tests of cold-formed steel compression members at elevated temperatures, *Steel and Composite Structures*, **14**(3), 205-227.

[26] Bicelli AA, Landesmann A, Camotim D, Dinis PB (2021). Flexural-torsional failure and DSM design of fixed-ended cold-formed steel columns at elevated temperatures, *Thin-Walled Structures*, **169**(December), paper 108362 (16 pages).

[27] Landesmann A, Camotim D, Silva FCM (2019). DSM design of cold-formed steel columns failing in distortional modes at elevated temperatures, *International Journal of Steel Structures*, **19**(3), 1023-1041.

Acknowledgements

The first two authors gratefully acknowledge the financial support of the Brazilian institutions (i) CAPES (Coordenação de Aperfeiçoamento de Pessoal de Nível Superior) – Finance Code 001, (ii) CNPq (Conselho Nacional de Desenvolvimento Científico e Tecnológico) – Finance Codes 141021/2020-9 and 13197/2020-2 and (iii) FAPERJ (Fundação Carlos Chagas Filho de Amparo à Pesquisa do Estado do Rio de Janeiro) – Finance Code E-26/200.959/2021 (second author). The third author gratefully acknowledges the financial support of FCT (Fundação para a Ciência e a Tecnologia – Portugal), through project UIDB/04625/2020 (funding the research unit CERIS).